DTU Library

Optimization under uncertainty of a biomass-integrated renewable energy microgrid with energy storage

Zheng, Yingying; Jenkins, Bryan M.; Kornbluth, Kurt; Træholt, Chresten

Published in:
Renewable Energy

Link to article, DOI:
10.1016/j.renene.2018.01.120

Publication date:
2018

Document Version
Peer reviewed version

Accepted Manuscript

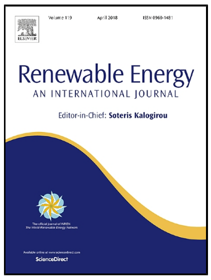

Optimization under Uncertainty of a Biomass-Integrated Renewable Energy Microgrid with Energy Storage

Yingying Zheng, Bryan M. Jenkins, Kurt Kornbluth, Chresten Træholt

PII:	S0960-1481(18)30130-7
DOI:	10.1016/j.renene.2018.01.120
Reference:	RENE 9725
To appear in:	*Renewable Energy*
Received Date:	17 May 2017
Revised Date:	28 December 2017
Accepted Date:	30 January 2018

Please cite this article as: Yingying Zheng, Bryan M. Jenkins, Kurt Kornbluth, Chresten Træholt, Optimization under Uncertainty of a Biomass-Integrated Renewable Energy Microgrid with Energy Storage, *Renewable Energy* (2018), doi: 10.1016/j.renene.2018.01.120

Optimization under Uncertainty of a Biomass-Integrated Renewable Energy Microgrid with Energy Storage

Yingying Zheng[a,*], Bryan M. Jenkins[a], Kurt Kornbluth[a], Chresten Træholt[b],

[a] Department of Biological and Agricultural Engineering, University of California, Davis, One Shields Avenue, Davis, Ca 95616, USA

[b] Department of Electrical Engineering, Technical University of Denmark, Elektrovej, 2800 Kgs. Lyngby, Denmark

Nomenclature

Abbreviations

MG	microgrid
CHP	combined heat and power
BCHP	biomass-based CHP
GS	biomass gasifier
ICE	internal combustion engine
WT	wind turbine
PV	photovoltaic
ES	energy storage
BT	battery
PGS	producer gas storage
TES	thermal energy storage
HOB	heat-only boiler
MCS	Monte Carlo simulation
COE	cost of energy
PDF	probability density function

Symbols

E	electricity demand (kWh)
H	heat demand (kWh)
Z	net acquisition cost ($)
P	purchase and installation (capital) cost ($)
O&M	operation & maintenance cost ($/kWh)
F	feedstock or fuel cost ($/kWh)
C	hourly capital cost ($/h)
M	rated capacity (kW)
N	expected life (years)
s	economic scaling factor
T	length of planning horizon (h)
V	set of all system components that contribute to capital cost
U	set of all system components that contribute to O&M cost
x	decision variable: hourly energy flow (kWh/h)

Superscripts and subscripts

t	time step (s)
p	actual facility

o	reference facility
i	index of installed units that contribute to capital cost
j	index of installed units that contribute to O&M and fuel cost
chr	charging
dis	discharging
min	minimum charging and discharging rate (kWh/h)
max	maximum charging and discharging rate (kWh/h)

Abstract

Deterministic constrained optimization and stochastic optimization approaches were used to evaluate uncertainties in biomass-integrated microgrids supplying both electricity and heat. An economic linear programming model with a sliding time window was developed to assess design and scheduling of biomass combined heat and power (BCHP) based microgrid systems. Other available technologies considered within the microgrid were small-scale wind turbines, photovoltaic modules (PV), producer gas storage, battery storage, thermal energy storage and heat-only boilers. As an illustrative example, a case study was examined for a conceptual utility grid-connected microgrid application in Davis, California. The results show that for the assumptions used, a BCHP/PV with battery storage combination is the most cost effective design based on the assumed energy load profile, local climate data, utility tariff structure, and technical and financial performance of the various components of the microgrid. Monte Carlo simulation was used to evaluate uncertainties in weather and economic assumptions, generating a probability density function for the cost of energy.

Keywords: microgrids, renewables integration, combined heat and power, biomass, modeling, energy storage, uncertainty, stochastic analysis

1. Introduction

Microgrids (MG) are smaller distribution networks usually installed close to the end users, and frequently contain hybrid energy resources, storage devices, and controllable loads. The traditional power grid is generally a large-scale centralized network where power plants generate high voltage electricity that is transferred and distributed to lower voltage end users. A significant fraction of electrical energy is dissipated in delivery due to the long distances between generator and load. Microgrids have been developed around the world as a means to address the high penetration level of renewable generation and reduce greenhouse gas emissions while attempting to address supply-demand balancing at a more local level [1].

The electricity generation of microgrid via solar PV and wind turbines depends, of course, on the total solar radiation and the wind speed in general. Due to the stochastic nature of these renewable energy resources, load behaviors, and market prices, a dispatchable generation unit is frequently included that can be turned on or off or modulated to adjust power output accordingly. The most common dispatchable units are diesel, natural gas, or biomass powered engine-generators. Moreover, an energy storage system is adopted in most cases to neutralize mismatch between generation and demand and tackle the uncertainty of demand forecasts. Energy storage provides the necessary means to shift the microgrid supply to a higher market price period based on the time of use. As an alternative to energy storage, load shifting can be applied to match demand with renewable energy generation. Load shedding may also be feasible, or other types of generation added to ensure demand is satisfied [2]. MG can also be operated with connection to the central power grid, in which case the central grid is used as a backup to reduce or eliminate the need for local storage, or while completely disconnected from the central grid or islanded [3]. When connected, the customer sometimes has the option of selling surplus electricity back to the utility grid operator under a net metering, feed-in, or other power purchase agreement.

In microgrid applications, both manufacturers and customers are interested to know the optimal capacity of the associated components of the system and the dispatch strategy to use in order to minimize cost and environmental impacts. Due to the computational complexity, a number of software packages have been developed to assist in microgrid design and assessment including HOMER [4-8] and DER-CAM [9-11]. Rohit et al. [12] proposed a hybrid off-grid system for a rural application with HOMER. Braslavsky et al. [13] presented an economic model of a shopping center, developed in DER-CAM, using on-site-specific demand, tariffs, and performance data for each technology option available.

Furthermore, substantial studies on microgrid optimal design and operation are typically formulated as minimization or maximization problem constrained by energy demand, capacity limits, ramping rate, and startup or shutdown times [14-21], and most address electricity only although thermal loads may also exist. Both thermal and electrical load profiles can fluctuate hourly and seasonally and utility tariff prices for natural gas and electricity may change dynamically as well. In these cases, electricity-led assumptions cannot guarantee an optimal solution overall. A number of modeling studies incorporating CHP units in the microgrid have considered both electricity and thermal demand [22-29] but few address biomass integration including separation of the fuel production and power generation components.

Variables that are subject to uncertainty in microgrid design and operation include unscheduled maintenance, climatic conditions (e.g. wind and cloudiness), and energy market prices and demands [30-40]. Model prediction control and receding horizon control (RHC) are frequently used to predict and make decisions under uncertainty [41-47]. Jiang and Fei addressed the problem of adopting multiple CHPs for cost reduction in microgrid using hierarchical optimization [48]. Xie et al. [49] developed a look-ahead optimal control algorithm for dispatching the generation units with the objective of minimizing both generation and environmental costs. Silvente et al. [50] used the RHC approach to analyze uncertainty in both energy generation and demand. Monte Carlo simulation (MCS) has been widely used to evaluate the reliability of a microgrid by generating data from fixed probability distributions of stochastic variables, such as wind speed, solar irradiance, customer demands, and others [51-55].

Currently most of the CHP integrated microgrid sizing and scheduling studies have assumed the CHP system as a single unit. However, where a fuel generation unit, such as a biomass gasifier, is deployed, producer gas production and electricity generation can also be treated as two separate and independent processes. The producer gas after biomass gasification can be used directly to fuel an internal combustion engine, microturbine, or another prime mover for power generation, and also used in a furnace or boiler for heat generation to offset utility natural gas demand [56]. Most studies considering energy storage include thermal storage or battery; separate gas storage is typically not considered, instead relying on pipeline supply as the storage equivalent and thereby subject to utility pricing. Biomass integrated models using RHC to schedule combined fuel gas generation and storage, engine cogeneration, auxiliary boiler and thermal energy storage operations have not previously been developed.

To address the above-mentioned issues, a model was developed to optimize the design and scheduling of an integrated biomass combined heat and power microgrid (BCHP-MG) system. The model combines a deterministic optimization module with a stochastic module and Monte Carlo simulation. Developing a more general model capable of solving for the optimal configuration and dispatch of a renewable energy microgrid with the flexibility of biomass integration was the primary objective for this work. Specifically, the objectives include: 1) finding the optimal capacity of wind and PV generation in each proposed scenario, 2) developing an optimal dispatch strategy between the various BCHP, wind turbine (WT), PV, battery (BT), producer gas storage (PGS), thermal energy storage (TES), and heat-only boiler (HOB) components of the microgrid and the main utility grid (electricity and natural gas) based on hourly energy demands and tariff rates, 3) estimating the effects of BT capacity on the cost of energy (COE) for different scenarios, 4) evaluating the influence of tariff rates and demand profiles on the COE and unit dispatch strategies, and 5) investigating the impact of stochastic variables on the final COE probability distribution.

2. Model development

2.1. Microgrid system design

For quantifying the analysis, microgrid systems with the following components are considered (Fig.1):

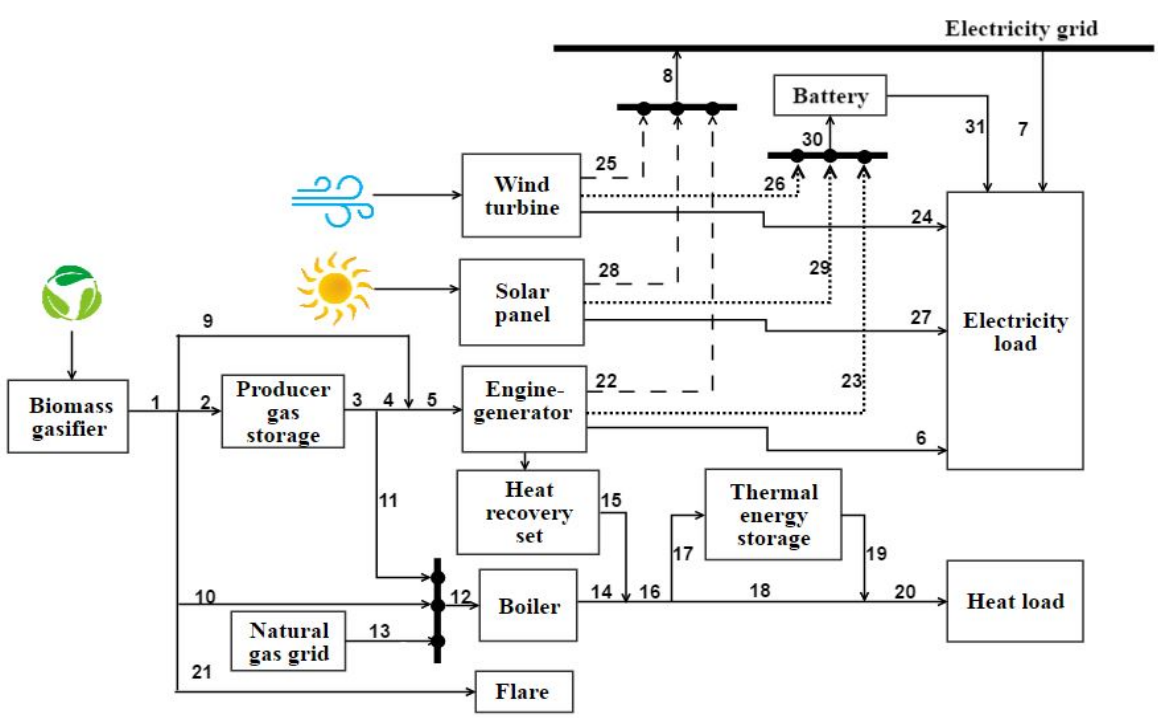

Fig. 1. Schematic microgrid system.

The electricity demand is met by the sum of the BCHP, WT, PV generation and the BT discharge, within their operating limits and constraints. The electricity generated via the PV array and WT depends on the solar radiation and the wind speed in general. The power from the BCHP, WT and PV modules is allowed to charge the BT, depending on the operating strategy selected. Producer gas from the BCHP unit is assumed to be purified and cooled, and can be used directly as fuel for the engine-generator sets and the boiler, stored in the producer gas storage tank, or simply flared for disposal if no economic demand exists and storage is at full capacity [57]. The PGS can be charged when the energy demand is low and discharge during high demand to improve system reliability. It can also be deployed to increase export electricity under a power purchase agreement to raise system revenue when the utility price is high if on a time of use tariff. For internal combustion reciprocating-type engines, heat for other uses can typically be recovered from the engine cooling jacket, exhaust, and potentially the engine surfaces in a combined heat and power mode. The recovered heat can be employed for a number of purposes, including direct heat utilization but also chilling, cooling, and additional electricity generation in a combined cycle mode although the latter is not included here. Similar to PGS, the recovered thermal energy can be used immediately or stored in a thermal energy storage system, in this case a warm water tank is assumed. The auxiliary HOB operates to make up any heat shortage, with heat otherwise supplied from producer gas burned directly from the gasifier, producer gas taken from storage (PGS), or utility natural gas.

For utility grid-connected scenarios, any electricity or heat supply deficits from the microgrid are satisfied by purchasing electricity or natural gas from the utility. In some circumstances surplus electricity from the microgrid is available for delivery to the utility under a net metering, feed-in tariff, or other power purchase arrangement generating revenue for the microgrid operation.

2.2. Microgrid component modeling

2.2.1. BCHP

BCHP is assumed to operate as a load following power plant and alter its output to meet varying demands within the capacity limit.

$$\mathrm{P_{BCHP}}(\mathrm{t}) = f(\mathrm{load}) \qquad (1)$$

In the case of BCHP, routine maintenance is required, but there is also the risk of unscheduled outages due to mechanical and other failures. In this study both the gasifier and engine are assumed to have a certain failure risk for unscheduled maintenance and would not be available for generation. The gasifier and engine failures are assumed to be independent, so that the gasifier or the engine may be available when the other fails. Both the gasifier and engine operation are treated as binary being either on (1) or off (0) with variable capacity when the units are on. The probability density function of the Bernoulli distribution is used to represent the stochastic nature of gasifier and engine.

$$\mathrm{f(O)} = \begin{cases} 1 & \text{for } \mathrm{P_f} \le \mathrm{x} < 1 \\ 0 & \text{for } 0 \le \mathrm{x} \le \mathrm{P_f} \end{cases} \qquad (2)$$

Where f (O) is the operating mode of the gasifier or engine (independent); P_f is the failure chance of gasifier or engine.

2.2.2. Wind turbine

Wind power generation depends on wind speed and the interference of the turbine with the wind. The output power of the turbine can be one of these three values [44]:

$$P_{wt}(t) = \begin{cases} 0 & \text{if } V(t) < V_{cutin} \text{ or } V(t) > V_{cutout} \\ \frac{1}{2} C_p \rho A_{wt} V(t)^3 & \text{if } V_{cutin} < V(t) < V_{rated} \\ \frac{1}{2} C_p \rho A_{wt} V_{rated}^3 & \text{if } V_{rated} < V(t) < V_{cutout} \end{cases} \tag{3}$$

Where P_{wt} is the mechanical output power of the turbine (W), ρ is air density (kg /m^3), A_{wt} is the turbine swept area (m^2), V is the undisturbed wind speed (m/s), C_p is the performance coefficient (or power coefficient) of the turbine, and V_{cutin}, V_{rated} and V_{cutout} are the cut in, rated, and cut out wind speed (m/s) of the turbine.

Probability density functions (PDF) were used to characterize the stochastic behavior of wind speed. The wind speed over a predefined time period was estimated using a Weibull PDF [55].

$$f(V) = \frac{k}{c}\left(\frac{V}{c}\right)^{k-1} \exp\left(-\left(\frac{V}{c}\right)^{k}\right) \tag{4}$$

$$k = \left(\frac{\sigma}{\mu}\right)^{-1.086} \tag{5}$$

$$c = \frac{\mu}{\Gamma\left(1 + k^{-1}\right)} \tag{6}$$

Where f(V) is the frequency rate of wind velocity; c is the Weibull scale parameter, a measure of the characteristic wind speed of the distribution; k is the Weibull shape parameter and specifies the shape of a Weibull distribution, taking on a value of between 1 and 3; μ is the mean wind speed (m/s) and σ is the standard deviation of the wind speed (m/s). The parameters k and c can be computed from μ and σ. A small value for k signifies highly variable winds, while constant winds are characterized by a larger k.

2.2.3. Photovoltaic module

The output power of the PV is given by the following equation [58] :

$$P_{pv}(t) = \eta_{pv} A_{pv} S \tag{7}$$

Where P_{pv} is the output power of the PV (W), $\boldsymbol{\eta}_{pv}$ denotes the conversion efficiency of the PV array (%) including the intrinsic module efficiency and array shading factor as appropriate, A_{pv} is the array area (m^2), and S is the solar radiation, treated as a random variable (W/m^2).

Solar irradiation is a stochastic variable that depends on the weather conditions and possible changes in shading throughout the day. Local shading or terrain effects that may also influence the resource availability are highly site-specific and not part of this analysis. The probabilistic nature of solar irradiance is considered to follow a beta PDF [59].

$$f(S) = \frac{\Gamma(\alpha+\beta)}{\Gamma(\alpha)+\Gamma(\beta)} S^{(\alpha-1)}(1-S)^{\beta-1}, \quad \alpha \geq 0, \beta \geq 0 \tag{8}$$

$$\beta = (1-\mu)\left(\frac{\mu(1+\mu)}{\sigma^2} - 1\right) \tag{9}$$

$$\alpha = \frac{\mu\beta}{1-\mu}$$

(10)

Where α and β are the function parameters and S is the horizontal solar irradiance (kW/m^2); α and β are calculated from the mean and standard deviation of solar irradiance μ and σ. Similar to the wind speed, an hourly average solar irradiance is used.

2.2.4. Energy storage

As an energy storage device, the battery storage injects power to the microgrid when the local generation is insufficient and absorbs power from the microgrid when the local generation is abundant or a model decision criterion indicates that saving the electrical energy for the future hours would increase net economic benefit. Producer gas storage can be charged when the producer gas production is abundant or a model decision criterion decides that storing the producer gas for future generation either as electricity or heat would improve the value of the objective function. Thermal energy storage was modeled as sensible heat storage, using water as the storage medium, and considering only energy flows through the warm water storage tank.

2.3. Mathematical formulation

2.3.1. Decision variables

Decision variables express the microgrid operating modes and the energy flows (kWh/h) between system components. The *x* variables define the energy flows throughout the microgrid system, each labeled with a subscript denoting the specific energy transfer (Fig. 1). The variables mentioned, along with other energy transfers, are now defined according to this notation. Each hour of the analysis involves 31 decision variables (Table 1).

Table 1 Decision variables.

Decision variables		Energy Flow from	Energy Flow in to
	x1	gasifier	
	x2	gasifier	gas storage
	x3	gas storage	
	x4	gas storage	engine
BCHP	x5		engine
	x6	engine	electricity demand
	x7	electricity grid	electricity demand
	x8		electricity demand
	x9	gasifier	engine

	x10	gasifier	boiler
	x11	storage	boiler
	x12		boiler
	x13	natural gas grid	boiler
	x14	boiler	
	x15	engine heat recovery	thermal demand
	x16	thermal production	
	x17	thermal production	thermal storage
	x18	thermal production	heating demand
	x19	thermal storage	heating demand
	x20		heating demand
	x21	gasifier	flare
	x22	engine	electricity grid
	x23	engine	battery
WT	x24	wind turbine	electricity demand
	x25	wind turbine	electricity grid
	x26	wind turbine	battery
PV	x27	solar panel	electricity demand
	x28	solar panel	electricity grid
	x29	solar panel	battery
BT	x30		battery
	x31	battery	electricity demand

2.3.2. Objective function

The optimization in this case is developed from the objective to minimize the cost of energy of over a particular time horizon (T) using an hourly time base. The objective function is formulated as:

$$\text{Min COE} = \frac{Z}{\sum_{t=1}^{T}\left(E_{load}^{t} + H_{load}^{t}\right)} \tag{11}$$

Where Z is the net energy supply cost ($); E_{load} and H_{load} are the electricity and heating demand (kWh); T is the length of the planning horizon (h) and t is the time step.

The net energy supply cost consists of the levelized fixed or capital costs of the system, the feedstock and fuel supply costs, and all operating and maintenance (O&M) costs, all resolved to a uniform cost of energy considering the time value of money. Capital and O&M costs in general are subject to economies of scale and hence influenced by the size of the units included in the system [60]. Feedstock and O&M costs assumed not to be subject to economies of scale although in practice pricing may depend on supply quantities.

$$Z = \sum_{t=1}^{T} \left(\sum_{i \in V} C_i^t + \sum_{j \in U} (O\&M_j^t + F_j^t) * x_j^t \right) \tag{12}$$

$$C_i = \frac{P_i}{8760} \frac{ir(1+ir)^N}{(1+ir)^N - 1}$$

(13)

$$\frac{P_p}{P_o} = \left(\frac{M_p}{M_o} \right)^s \tag{14}$$

Where V is the set of all installed system components that contribute to capital cost; i is the index for all the installed units that contribute to capital cost; U is the set of all energy flows that create O&M and fuel cost; j is the index for the energy flows that create O&M and fuel cost; C is the hourly levelized capital cost ($); O&M and F are the hourly O&M and fuel cost of energy flow j at time t ($/kWh); x is the energy flow (kWh); P is the overnight purchase and installation cost that is influenced by an economy of scale defined by the value of s ($0 \leq s \leq 1$) [61]; ir is the interest rate, and N is expected life time (y). The constant 8760 is the conversion for the number of hours per year and is uncorrected for leap years. For the equation defining the economy of scale, P_p is the capital cost of facility or unit under consideration within the microgrid; P_o is the known capital cost of a reference facility or unit of the same type, M_p is the rated capacity of the unit under consideration; M_o is the rated capacity of the reference unit.

2.3.3. Constraints

All energy flows ($x_{1\text{-}31}$) are signed with lower (zero) and upper bounds with the latter being the maximum acceptable capacities. The electricity balance constraints the electrical demand to be satisfied by BCHP, WT, PV, BT or the grid power. The heat balance constraints the heating demand to be satisfied by the producer gas powered boiler, the natural gas powered boiler, the heat recovered from engine generator set, or some combination of these sources. Therefore, the energy balances at time t for the microgrid can be written as follows:

$$x_6^t + x_7^t + x_{24}^t + x_{27}^t + x_{31}^t = E_{load}^t \tag{15}$$

$$x_{20}^t = H_{load}^t \tag{16}$$

The BT and PGS storage levels at the current time step t depend on the storage level at previous time step (t-1) and the current charging or discharging rate. The BT and PGS energy balances are:

$$BT^t = BT^{t-1} + x_{30}^t - x_{31}^t \tag{17}$$

$$PGS^t = PGS^{t-1} + x_2^t - x_3^t \tag{18}$$

Where BT^t and PGS^t are the energy storage level at current time step t, BT^{t-1} and PGS^{t-1} the amounts of energy stored in BT and PGS at previous time step t-1.

Storage level constraints require that storage levels should be in the range between the minimum and maximum determined safety and economy. The constraints of charging and discharging indicate the changing rate for BT and PGS should be within the upper and lower limits. The maximum charge and discharge rate is for the model developed here assumed to be half of the rated capacity. The charging and discharging efficiencies of BT and PGS are assumed small although this is not a general constraint of the model. The constraints for TES are as same as BT and PGS.

$$BT_{min} \leq BT^{t} \leq BT_{max} \quad (19)$$

$$BT\_chr_{min} \leq x_{30}^{t} \leq BT\_chr_{max} \quad (20)$$

$$BT\_dis_{min} \leq x_{31}^{t} \leq BT\_dis_{max} \quad (21)$$

$$PGS_{min} \leq PGS^{t} \leq PGS_{max} \quad (22)$$

$$PGS\_chr_{min} \leq x_{2}^{t} \leq PGS\_chr_{max} \quad (23)$$

$$PGS\_dis_{min} \leq x_{3}^{t} \leq PGS\_dis_{max} \quad (24)$$

Where BT_{min} and BT_{max} are the minimum and maximum allowed BT energy storage level at any time, and the same goes for PGS; chr_{max} and dis_{max} are the maximum allowed charging and discharging rates; chr_{min} and dis_{min} are the minimum allowed charging and discharging rates.

The power ramping constraint, expressed in kWh per hour, indicates how much a generator can change its output between two successive time steps.

$$|x_{1}^{t} - x_{1}^{t-1}| \leq G\_ramp_{rate} \quad (25)$$

$$|x_{6}^{t} - x_{6}^{t-1}| \leq E\_ramp_{rate} \quad (26)$$

Where x_1 is the biomass gasifier production at time t; x_6 is the ICE production at time t; G_ $ramp_{rate}$ and E_ $ramp_{rate}$ are the ramping rates of the gasifier and the engine-generator, which is related to the capacity and type.

Some decision variables are coupling with each other and constrained by energy balance, for example:

$$x_{1}^{t} = x_{2}^{t} + x_{9}^{t} + x_{10}^{t} + x_{21}^{t}$$

(27)

Where x_2, x_9, x_{10}, and x_{21} represents the energy flow out of biomass gasifier to either gas storage, engine, boiler, or flare, respectively (Table 5). Similar energy balance constraints are shown in Fig. 1.

This mathematical formulation of the system design and unit commitment problem is a linear convex optimization problem. The model implementation was here solved using MATLAB with its optimization toolbox (MATLAB 2016a, Mathworks, Natick, Massachusetts).[1]

[1] mention of a specific tradename does not constitute an endorsement by the University of California.

2.4. Solution method

The model discussed here chains a deterministic planning optimization module with a stochastic module (Fig. 2).

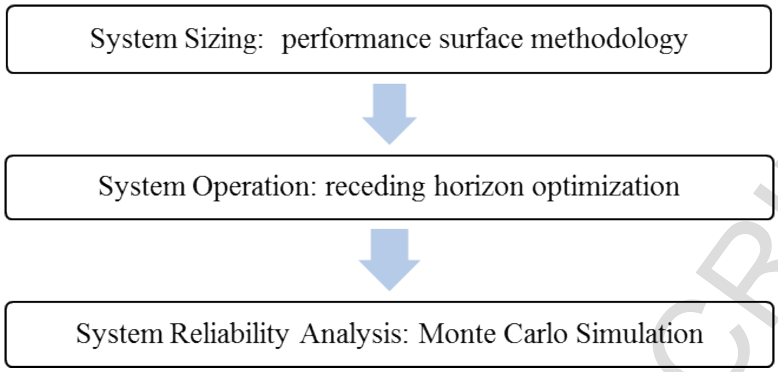

Fig. 2. Microgrid optimization modules.

2.4.1. Performance surface method

The model is first solved deterministically to derive the optimal wind and solar capacities for each proposed microgrid scenario. The capacity of WT and PV units is gradually increased from none to 250 kW (with 10 kW of increment) in a search for the optimal capacity yielding minimum cost with the rest of units fixed. The criterion of selecting the best hybrid energy system combination for a proposed site is based on minimizing the cost for different renewable combinations, the output of the optimal sizing and operation being the preferred set of WT and PV modules. The entire procedure is repeated for all the possible combinations. The combination with the lowest cost overall is selected as optimal design for each scenario.

2.4.2. Sliding time window

Once all the unit capacity has been fixed, the dispatch of the available units to meet demand at the lowest cost is required. The hourly operation strategy of the different hybrid configurations is determined by using linear constrained optimization. The sizing and operating strategies are interdependent so a different set of component configurations is analyzed in each hybrid combination to find the optimal hybrid system.

A sliding time window method is used to first determine the optimal operation of all microgrid components [43, 50]. For the examples included here, a 4-hour time window is used with known electrical and heat demand. Each hour has a total of 31 solution variables (Fig. 1), which for a 4-hour horizon requires solving for 124 variables. Within each time window, linear optimization is applied to obtain the gasifier, gas storage, engine, boiler, thermal storage, WT, PV and BT operation giving the minimum operating cost. Only the solution for the first hour is retained to compute the actual generation and cost. At the same time, the new initial conditions of all the energy storage devices including the BT, PGS, TES units are updated. The time window is then incremented by one hour, and the process repeated for the entire time horizon (27 hours for a 24 hour period). The sliding time window approach is summarized in the following steps (Fig. 3).

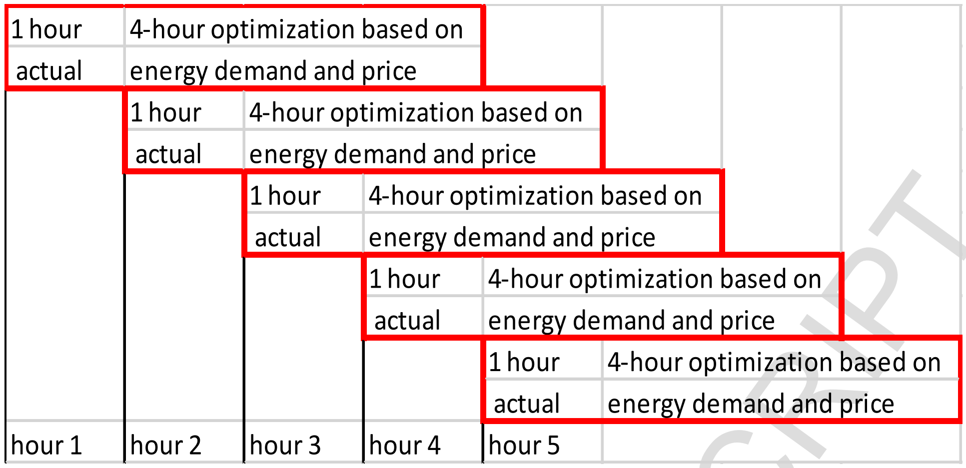

Fig. 3. Sliding window method (4-hour window illustrated over a period of 5 hours).

1. Specify initial conditions of energy storages.
2. Optimize the system operation as outlined above for the period from t_initial to t_initial+ T (T: sliding time window width).
3. Obtain the optimal operating points of all units.
4. Set the operating conditions of the first hour of the window to the optimal conditions.
5. Update energy storage conditions.
6. Slide the window 1 hour forward in time.
7. Repeat from step 2.

2.4.3. Monte Carlo simulation

Monte Carlo simulation was conducted to generate a finite number of possible outcomes based on the probability distributions of assumed stochastic parameters. A total of 1000 Monte Carol simulations were used to generate the cost of energy distributions for each scenario. The distribution of simulated outcomes for the 1000 realizations of the COE provided the risk profile.

3. Model application

3.1. Case study definition

The input data for the model were divided into the following categories: 1) customer information (load profile and weather data), 2) technical information (physical characteristics and specifications of all units, efficiency, heat to power ratio, power generation PDF, etc.), 3) financial information (capital cost, O&M cost, fuel costs, tariff rate). In the deterministic model, the output of the model is the optimal microgrid design and dispatch (based on the COE values). In the stochastic model, the output of the model is the probability distribution of COE.

For the case study located in Davis, California, a typical winter daily residential electricity load profile from the local utility was scaled up and used for analysis. A winter daily thermal demand profile from the UC Davis campus was scaled down to represent thermal energy usage (Fig. 4). The studied microgrid scale is around 100 kW. Therefore, the input load profiles are scaled up or down to the desired range. For the scenario analyses, the peak and base load demand for electricity and heating were in the range of 72-200 kW and 50-172 kW, respectively. Davis hourly solar and wind data in February were obtained from the California Irrigation Management Information System (CIMIS).

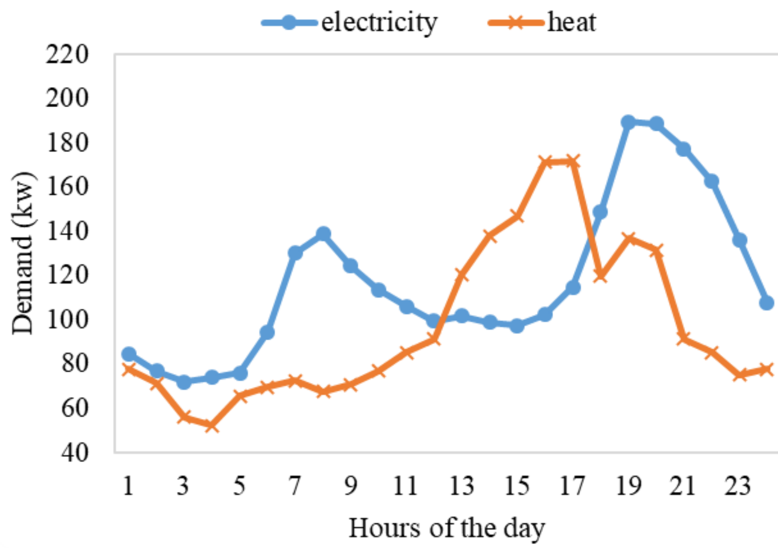

Fig. 4. Model hourly electricity and heat demand for February in Davis, California.

Technical and economic parameters for the wind turbines and PV assumed here are based on a 10 kW unit capacity. The efficiency and cost of the power converters have been included in the overall PV and wind turbines' efficiencies and costs. All parameters assumed for BCHP is based on a 100 kW unit capacity. All units are assumed to subject to 20 years life time and 6% of interest rate (Table 2).

Table 2 Technical parameters and cost assumptions for components of the microgrid [62-65].

	Parameters	**Unit**	**Value**
All units	Discount/interest rate	%	6
	Economic life	years	20
	Economic scale factor	-	0.9
BCHP	Rated power	kW	100
	Capital cost	$/kW	4500
	O & M cost	$/kWh	0.03
	Feedstock cost	$/kWh	0.02
	Electricity efficiency	-	0.3
	Heat recovery factor	-	0.6
WT	Reference module rated power	kW	10
	Reference module rotor diameter	m	7
	Capital cost	$/kW	2154
	O & M cost	$/kWh	0.005
	Fuel cost	$/kWh	0
	Cut-in wind speed	m/s	2.5
	Cut-off wind speed	m/s	50

	Rated wind speed	m/s	11
	Air density	kg/m^3	1.23
	Betz Coefficient	-	0.593
PV	Reference module rated power	kW	10
	Reference module surface area	m^2	64
	Capital cost	$/kW	3463
	O & M cost	$/kWh	0.005
	Fuel cost	$/kWh	0
	Electricity efficiency	-	0.2
BT	Rated capacity	kWh	200
	Capital cost	$/kWh	255
	O & M cost	$/kWh	0
	Round trip efficiency	-	0.9
PGS	Rated capacity	kWh	200
	Capital cost	$/kWh	80
	O & M cost	$/kWh	0.005
	Round trip efficiency	-	1
HOB	Rated power	kW	150
	Capital cost	$/kW	120
	O & M cost ($/kWh)	$/kWh	0.005
	Efficiency	-	0.85

Both capital and operating costs are also subject to uncertainty. An assumption was made here that all the capital and O&M costs are uniformly distributed over the range from zero to twice the reference cost, the lower bound representing an extreme incentive case with a high subsidy. The gasifier and engine are both assumed to have 5% of failure risk for unscheduled maintenance and would not be available for generation. The shape and scale factors for Weibull and Beta distribution are estimated by the curve fitting function in Matlab based on historical wind speed and solar irradiance data. Table 3 lists the 13 uncertainty parameters and their associated PDFs.

Table 3 Stochastic parameters and assumed PDF.

Stochastic parameter	PDF	PDF specifications
BCHP Capital cost ($/kW)	Uniform	[0,9000]
WT Capital cost ($/kW)	Uniform	[0,4308]
PV Capital cost ($/kW)	Uniform	[0,6926]
BT Capital cost ($/kW)	Uniform	[0,510]
GS O&M cost ($/kWh)	Uniform	[0,0.04]
ICE O&M cost ($/kWh)	Uniform	[0,0.02]
WT O&M cost ($/kWh)	Uniform	[0,0.01]

PV O&M cost ($/kWh)	Uniform	[0,0.01]
BT O&M cost ($/kWh)	Uniform	[0,0.002]
Wind speed (m/s)	Weibull	Shape factor k=1.6337; scale factor c=2.7813
Solar irradiance (w/m^2)	Beta	Shape factor a=0.0058; scale factor b=0.070
GS availability	Bernoulli	$P_f = 0.05$
ICE availability	Bernoulli	$P_f = 0.05$

For TOU rates, the price of electricity changes by time of day (Table 4). For natural gas, the price is assumed to be constant throughout the day. The electricity buyback price is assumed to be $0.04/kWh based on the net surplus compensation rate approved by the California Public Utilities Commission (CPUC) [66].

Table 4 Electricity tariff rate

Energy Source	Category	Tariff rate ($/ kWh)	Time
Electricity Buy	off-peak	0.22	00:00-09:59 am; 09:00-11:59 pm
	partial-peak	0.30	10:00-11:59 am; 07:00-08:59 pm
	peak	0.40	12:00-06:59 pm
Electricity Sell	all day	0.04	N/A
Natural gas Buy	all day	0.08	N/A

Five design configuration scenarios were selected to investigate various aspects of the biomass integrated microgrid optimization (Table 5). All are utility grid interconnected, installed with a 200 kW HOB and a 200 kWh TES. A net energy metering agreement is included with compensation for surplus electricity delivered from the microgrid to the utility. BCHP, PV and WT are allowed for connection to a utility meter. Scenario 1 includes only wind and PV generation with battery storage. This option is a good alternative for locations with very limited heat demand but abundant wind and solar resources, or areas without abundant biomass resources. Scenario 2 includes all the all three renewable sources but without producers gas storage. Scenario 3 also includes all three renewable sources with a full complement of producer gas, thermal, and battery storage but the biomass component is insufficient to meet peak load by itself. Scenario 4 is the same as Scenario 3 but with added BCHP capacity, in this case a duplicate unit for a total biomass generation of 200 kW, slightly higher than peak load. Scenario 5 is the presumed conventional system and supplies energy demands entirely from the utility electricity and natural gas grids.

Table 5 System components of the 5 proposed scenarios (●=unit included, x=unit excluded).

Scenario	BCHP_1	BCHP_2	WT	PV	PGS	BT
1	x	x	●	●	x	●
2	●	x	●	●	x	●
3	●	x	●	●	●	●
4	●	●	●	●	●	●
5	x	x	x	x	x	x

3.2. Deterministic model results

3.2.1. Optimal microgrid design

The lowest COE was found among all the possible combinations of WT and PV modules (WT: 0-250 kW; PV: 0-250 kW) (Table 6).

Table 6 Optimal system combinations.

Scenarios	System Configuration	Optimal WT Installed units	Optimal PV Installed units
1	BCHP (0), PGS (0), BT (200)	180	170
2	BCHP (100), PGS (0), BT (200)	0	160
3	BCHP (100), PGS(200), BT(200)	0	160
4	BCHP (200), PGS(200), BT(200)	0	130
5	BCHP (0), PGS(0), BT(0)	N/A	N/A

Figs.5-8 illustrate the 3D surface of cost response as a function of the capacities of WT and PV for scenarios 1 to 4. The optimum WT and PV capacity can be found around the minimum points in the figures. For scenario 1, when no BCHP is considered, the model yields the lowest cost with 180 kW of wind capacity and 170 kW of PV capacity. For scenarios 2, 3 and 4, when BCHP is included, no wind capacity is adopted for the cost structure assumed. The reference installed capital cost for PV was assumed to be \$3165/kW with \$0.005/kWh for O&M; for wind, the reference capital cost was \$2175/kW with \$0.005/kWh for O&M. Although the wind is assumed to have a lower capital cost, the wind speed profile for the site selected (Davis, California) has only 9 hours of the day with speeds above 2.5 m/s, the cut-in wind speed. Hence, generation is low and generation cost exceeds that of PV. From an economic viewpoint, PV and BCHP are the most attractive technology for this site under these cost assumptions. The optimal outcomes will in general differ depending on location. Comparing scenarios 2 and 3, no change in installed PV capacity is associated with the addition of producer gas storage. For scenario 4, with an oversized 200 kW BCHP, the optimal PV capacity declines to 130 kW.

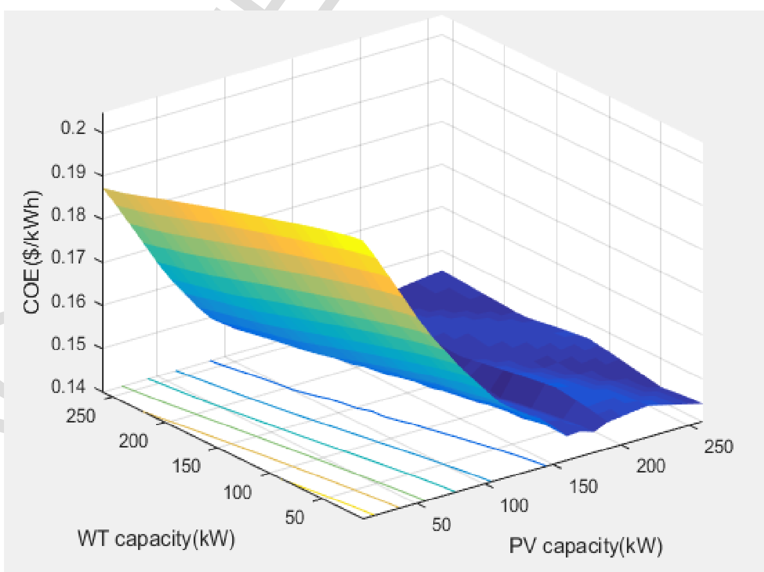

Fig. 5. COE surface of scenario 1 as a function of WT and PV capacities.

405 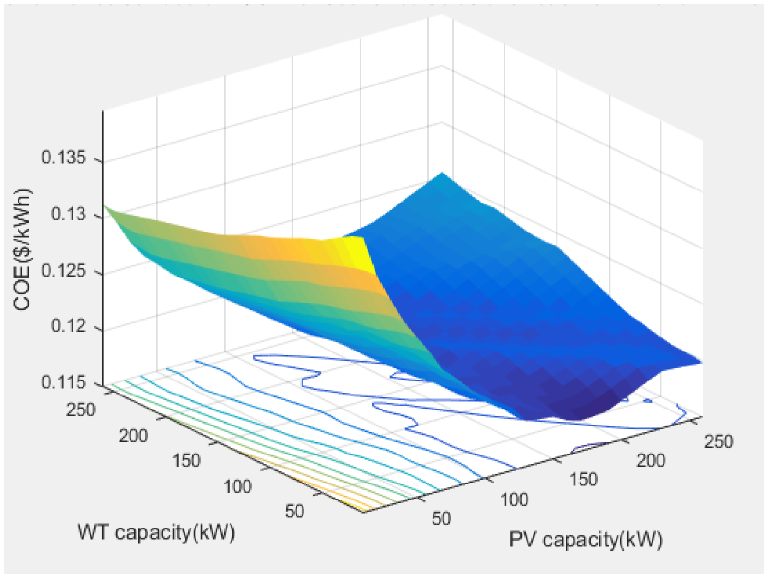

406 Fig. 6. COE surface of scenario 2 as a function of WT and PV capacities.

407 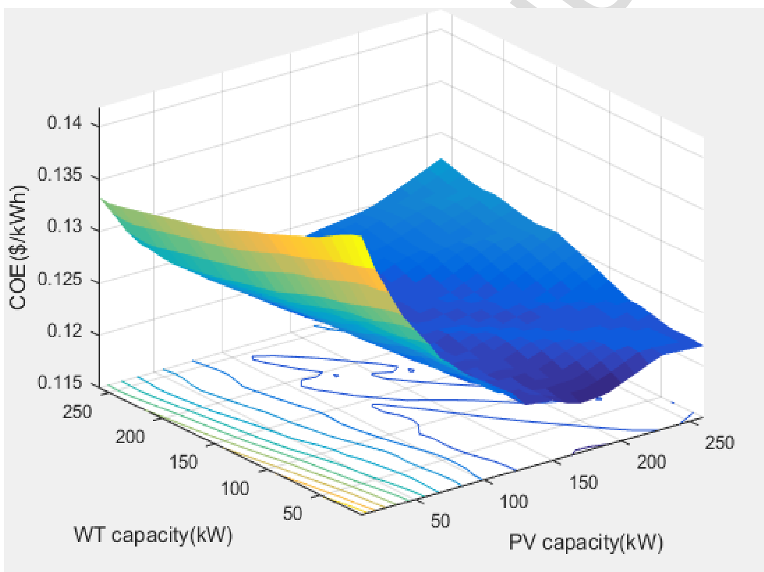

408 Fig. 7. COE surface of scenario 3 as a function of WT and PV capacities.

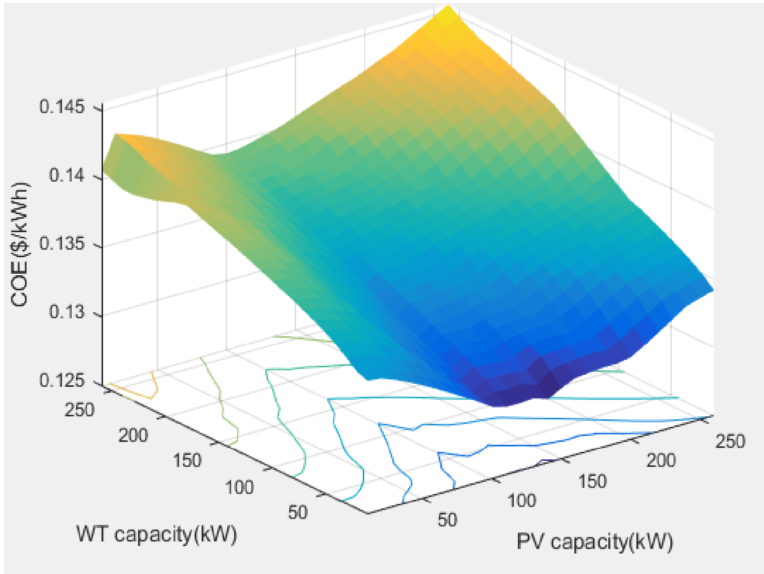

Fig. 8. COE surface of scenario 4 as a function of WT and PV capacities.

For the assumptions used in these examples, the total cost of the optimal system configuration varies from a low of $0.1182/kWh for Scenario 2, the 100 kW BCHP with 200 kWh battery storage scenario, to a high of $0.2029/kWh for Scenario 5, the utility only supply scenario. Scenario 4, with a 200 kW BCHP capacity and 130 kW of PV achieves 100% renewable supply through the microgrid with no utility purchase, but is higher in generation cost than the hybrid microgrids of Scenarios 2 and 3 relying on both microgrid and utility generation. Because of the boiler's installation, there is also installation cost in scenario 5 (Table 7).

Table 7 Optimal COE values and cost composition for 5 scenarios.

Composition of total cost ($)	scenario 1	scenario 2	scenario 3	scenario 4	scenario 5
Installation	239.75	259.91	263.37	334.94	7.70
O&M+Fuel	19.44	276.51	281.33	342.99	11.60
Electricity purchase	290.26	55.18	55.18	0.00	804.42
Natural gas purchase	218.44	28.44	28.45	0.00	218.44
Net metering credit	-16.48	-12.77	-10.95	-5.01	0.00
Daily total cost	751.40	607.27	617.37	672.91	1042.16
COE ($/kWh)	**0.1462**	**0.1182**	**0.1202**	**0.1310**	**0.2029**

Fig. 9 illustrates the economic results for the proposed 5 scenarios. Even with additional capital and installation costs, the introduction of BCHP reduces the need for electricity and natural gas purchases, and the overall total cost and COE are decreased through this on-site generation. In addition, the producer gas storage does not lead to obvious economic gains, due to the low cost assumed for purchased natural gas.

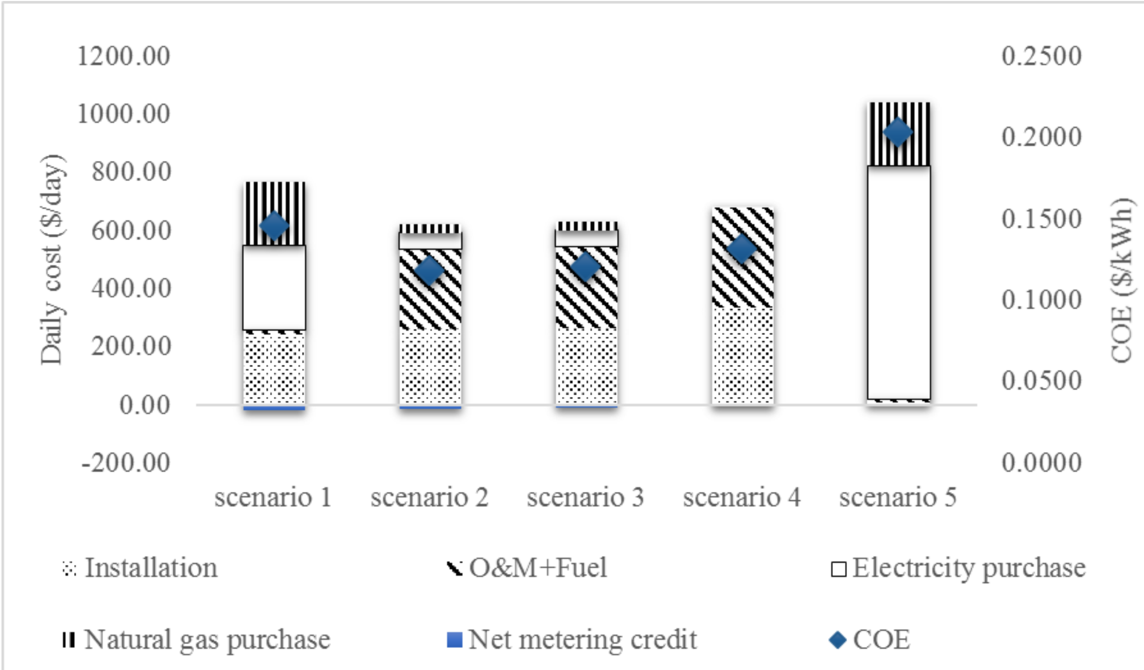

Fig. 9. COE values and cost composition for various scenarios.

To evaluate the effect of demand patterns from other times of the year on the optimal microgrid configuration, the model was also tested using daily electrical and thermal load data for summer. The lowest cost, $0.1136/kWh, is also found for scenario 2 employing the 100 kW BCHP with solar PV and battery storage. Scenario 1, with a 170 kW wind turbine capacity and 130 kW of PV achieves a COE of $0.1349/kWh, which is lower than the COE of scenario 1 in winter. That is because the heating demand is much lower in summer and the influence from the absence of a heat source in scenario 1 is minimized. For the same reason, the COE of scenario 4, with a 200 kW gasifier, is $0.1390/kWh in summer, which is higher compared to the COE in winter.

3.2.2. Optimal microgrid dispatch

Figs. 10-13 illustrate the optimal energy flows from the BCHP, WT, PV, and BT units as well as the grid to the demand during the selected 24 hour period. These graphs show the optimal dynamic operation based on the cost minimization.

For scenario 1, when no BCHP is adopted, most of the electricity during midnight to early morning is supplied by purchasing electricity from the utility due to the absence of PV generation and low wind speed (<2.5 m/s) for the data set selected. The morning peak load demand occurs between 07:00 to 09:00 am coinciding with an increasing time of use tariff; therefore, the BT is used to balance the demand in conjunction with PV. From 10:00 am to 16:00 pm, all of the electricity is generated from PV. After 07:00 pm, PV generation declines while as does the wind generation and import of grid power again increases to meet the nighttime demand (Fig.10).

Scenarios 2 and 3 show similar optimal operating schedules except for the addition of the BCHP that carries most of the demand not met by PV. Grid electricity is purchased after 20:00

when both BT reserve is depleted, PV is absent and the residual demand exceeds the 100 kW supply from the BCHP unit (Figs. 11-12).

Scenario 4 considers the case of having an oversized BCHP (200 kW) in the microgrid. In this case the BCHP is large enough to meet virtually all the nighttime demand when lower cost PV generation is absent with the exception of a small contribution from the battery in the later evening. No grid power is purchased and the microgrid independently meets the full system demand (Fig. 13).

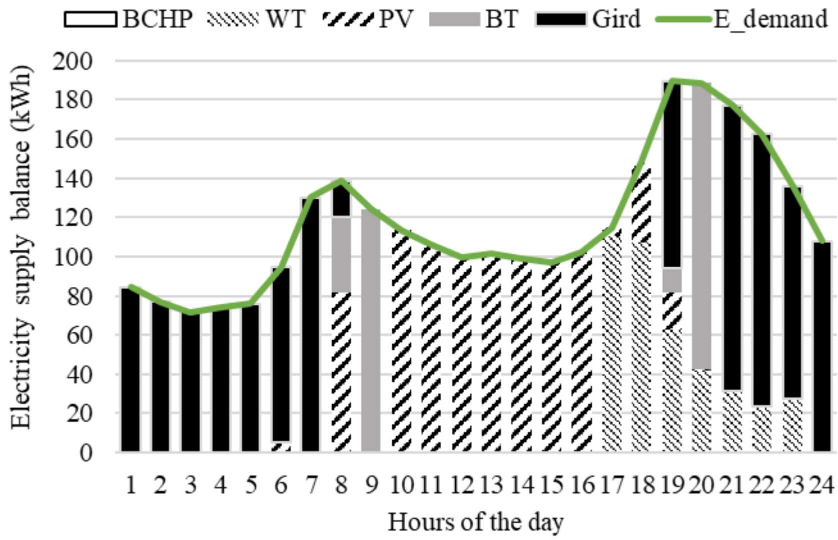

Fig. 10. Optimal electricity supply for scenario 1.

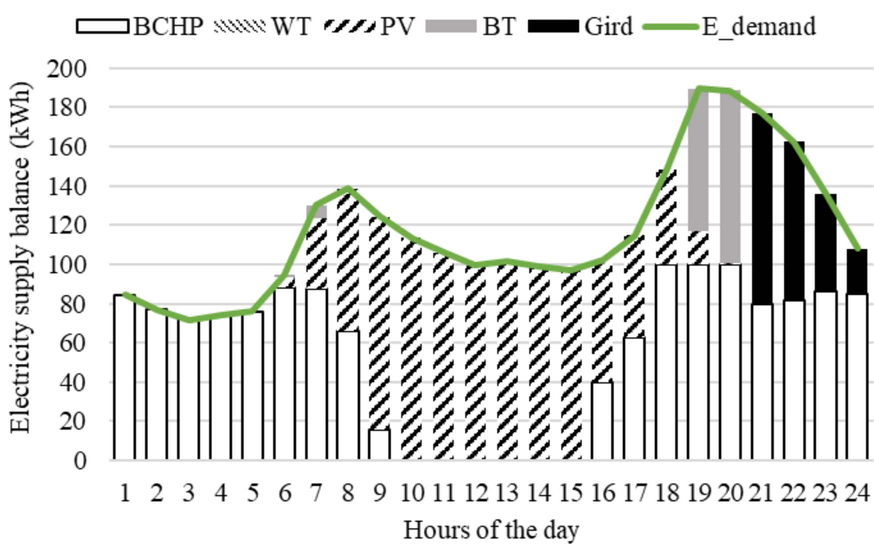

Fig. 11. Optimal electricity supply for scenario 2.

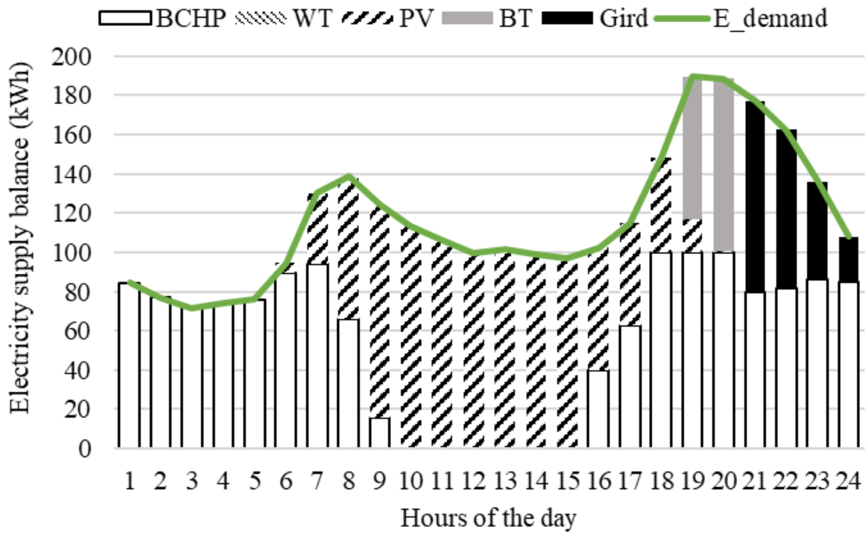

Fig. 12. Optimal electricity supply for scenario 3.

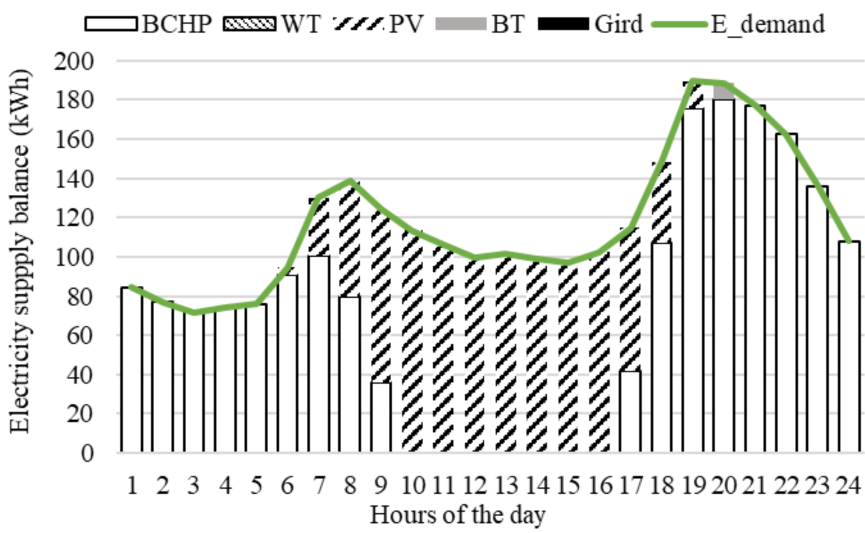

Fig. 13. Optimal electricity supply for scenario 4.

3.3. Sensitivity analyses

Sensitivity analyses were performed on BT capacity, electricity and natural gas prices, and energy demands. The analysis was based on the results obtained from the most optimistic WT and PV capacities giving the lowest cost.

3.3.1. Effects of battery capacity

To study the effect of battery capacity on the COE, the battery energy storage was varied from 0 to 300 kWh. The upper limit corresponds to the storage size of charging the battery with 100 kWh/h for 3 h. Because the sliding time window width is 4 h, the BT should be able to store at least 3 h of production. Fig. 14 illustrates COE as a function of the battery size for the 4 scenarios with the optimal capacity of WT and PV. For scenarios 1, 2 and 3, the COE decreases as the storage size increases. The larger the storage, the less purchased electricity is required by the customer during the higher tariff period. At approximately 125 kWh, the COE begins to increase due to the limitation of the gasifier capacity. With increasing length of the prediction window, part of the storage capacity becomes redundant. For example, if with an 80 kW engine-generator set and a 12 hours sliding time window, even if 100% of the model generation is stored over the first 11 hours, the optimal BT capacity will not be 880 kWh, but instead will be something less to still meet the demand over the model interval.

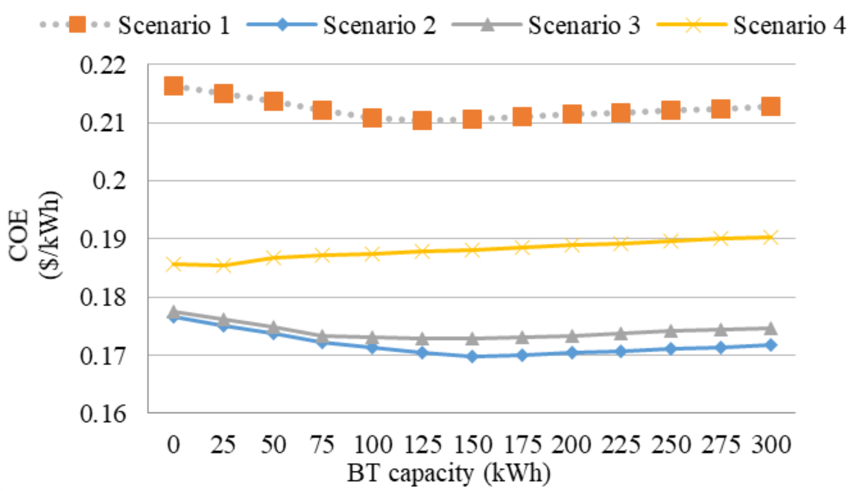

Fig. 14. COE as a function of battery capacity.

3.3.2. Effects of electricity and natural gas price

Fig. 15 and Fig. 16 show the results for the cost reduction ratio obtained by changing the electricity and natural gas price from 60% below to 60% above the reference prices. The microgrid provides greater cost savings as the price of purchased electricity increases (Fig. 15). However, the marginal benefit of having the microgrid declines with increasing grid price. A breakeven point is found for scenarios 1 and 4 at grid prices that are 55 and 45% lower than the assumed base case or reference price (negative cost reduction ratios indicate a preference for utility grid purchase). Moreover, although scenario 4 has the lowest cost savings at lower grid prices, as the grid price increases this scenario eventually achieves the same savings as scenarios 2 and 3 and breaks even with scenario 1 at a grid price about 20% lower than the reference price. If the electricity price is reduced more than 20%, the no-BCHP case, scenario 1, is preferred. As the purchased electricity price continues to increase, the larger BCHP capacity becomes more attractive.

For scenario 1, as natural gas price changes from 60% below to 60% above the reference price, the COE cost reduction ratio decreases from 32% to 25% due to the lack of heat recovery from a BCHP unit (Fig. 16). For scenarios 2, 3 and 4, the BCHP heat recovery and producer gas can almost meet the full heat demand, therefore, increasing natural gas price does not influence the COE reduction ratio and a nearly positive linear relationship develops over the remainder of the cost range.

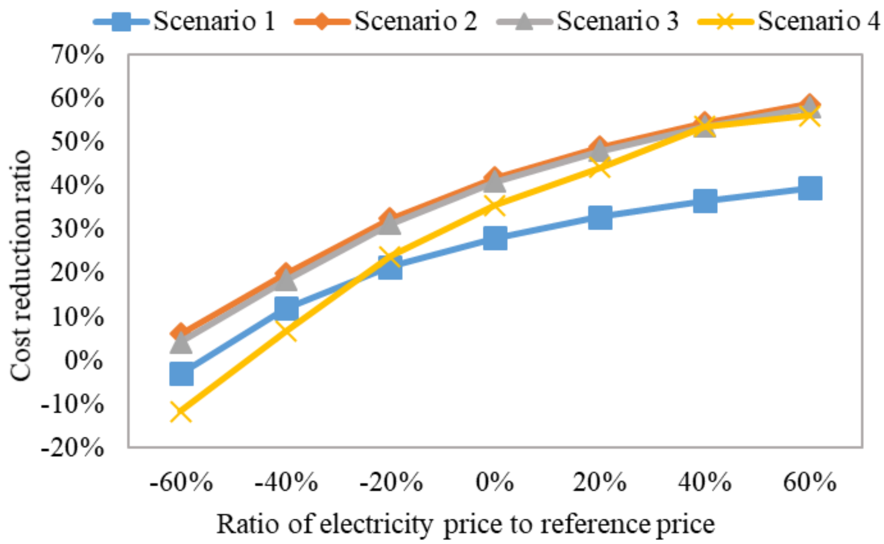

Fig. 15. COE reduction ratio as a function of increased electricity price.

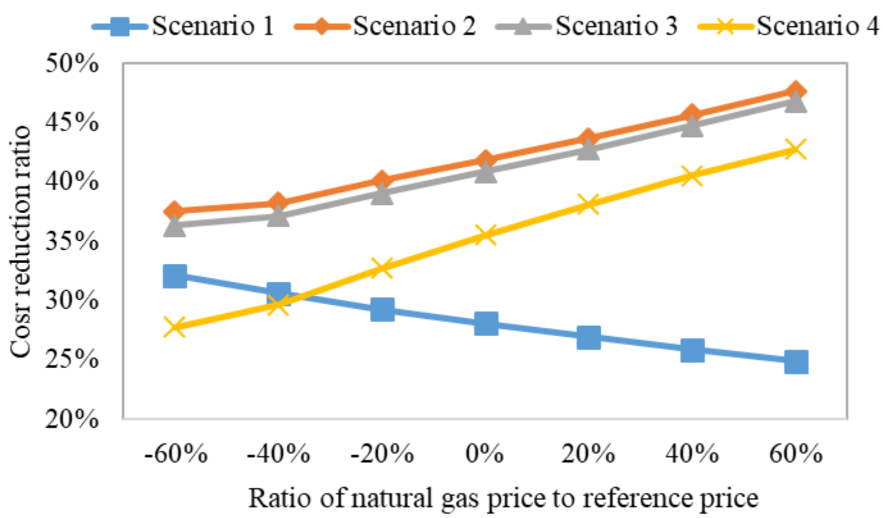

Fig. 16. COE reduction ratio as a function of increased natural gas price.

3.3.3. Effects of demand changes

Fig. 17 and Fig. 18 show the results for the cost reduction ratio obtained by changing the electricity and heat demand from 60% below to 60% above the reference values. The model yields a maximum cost reduction at around a 20% increase in the base electricity demand. At this demand level, the microgrid capacity is fully utilized for an overall improvement in cost of generation (Fig. 17). For the case of no BCHP or only a single BCHP unit is installed, the cost reduction ratio decreases slightly as the heat demand increases (Fig. 18). The overall impact on the COE is minor for scenarios 2 and 3, however, because the only heat resource in the microgrid is from BCHP (no electric resistance heating), which is absent in scenario 1, the COE becomes more sensitive to heat demand. For scenario 4, with 200 kW BCHP capacity, even when the heat demand is increased by 60% and the peak load is slightly over 200 kW, the microgrid still supplies most of the thermal energy from engine heat recovery and the boiler. Therefore, increasing the heat demand does not require much additional natural gas and a positive relationship results in contrast to that for scenario 1.

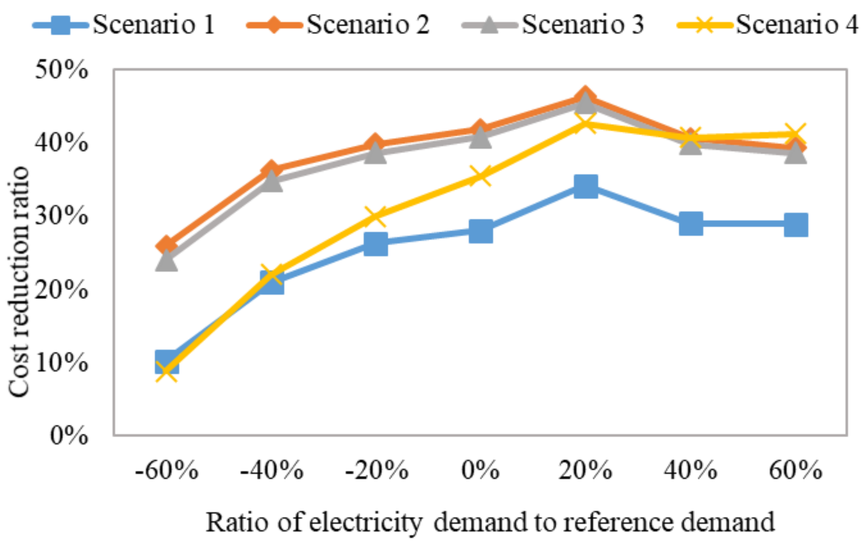

Fig. 17. COE reduction ratio as a function of increased electricity demand.

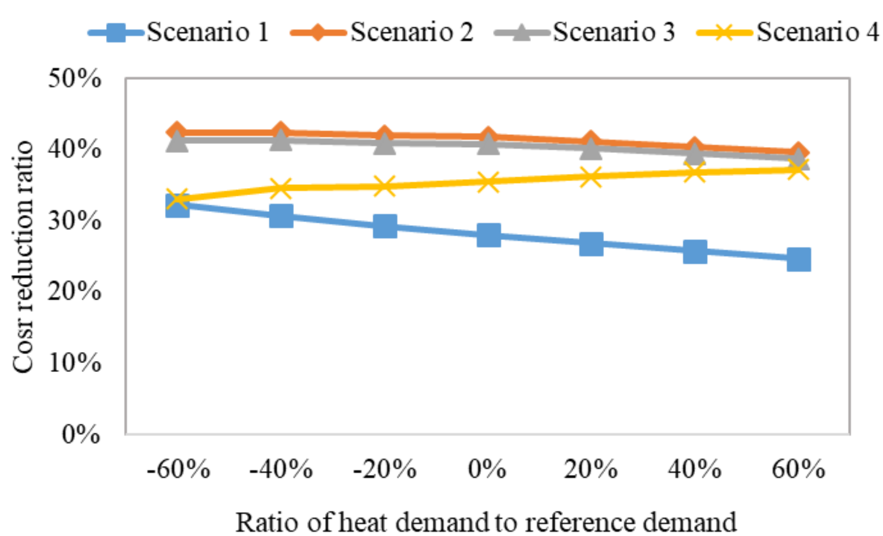

Fig. 18. COE reduction ratio as a function of increased heat demand.

3.4. Stochastic model results

Many of the technical and economic assumptions used in the model are subject to uncertainty as well as variability. To assess the potential risk associated with decisions around a particular microgrid design, a stochastic model was developed employing Monte Carlo simulation for COE. Histograms from the Monte Carlo simulations are presented in Fig. 19. The BCHP scenario distributions (scenarios 2-4) are centered at lower COE even with a 5% possibility of the gasifier and/or engine failure than for the microgrid without BCHP (scenario 1).

The 200 kW BCHP case (scenario 4) shows the widest variation in COE with cost mostly ranging between 0.01 and 0.26 $/kWh, a width of $0.25/kWh while the scenario 2 and 3 span about $0.17/kWh. The no BCHP case (scenario 1) shows the narrowest variation in COE around the mean of $0.13/kWh.

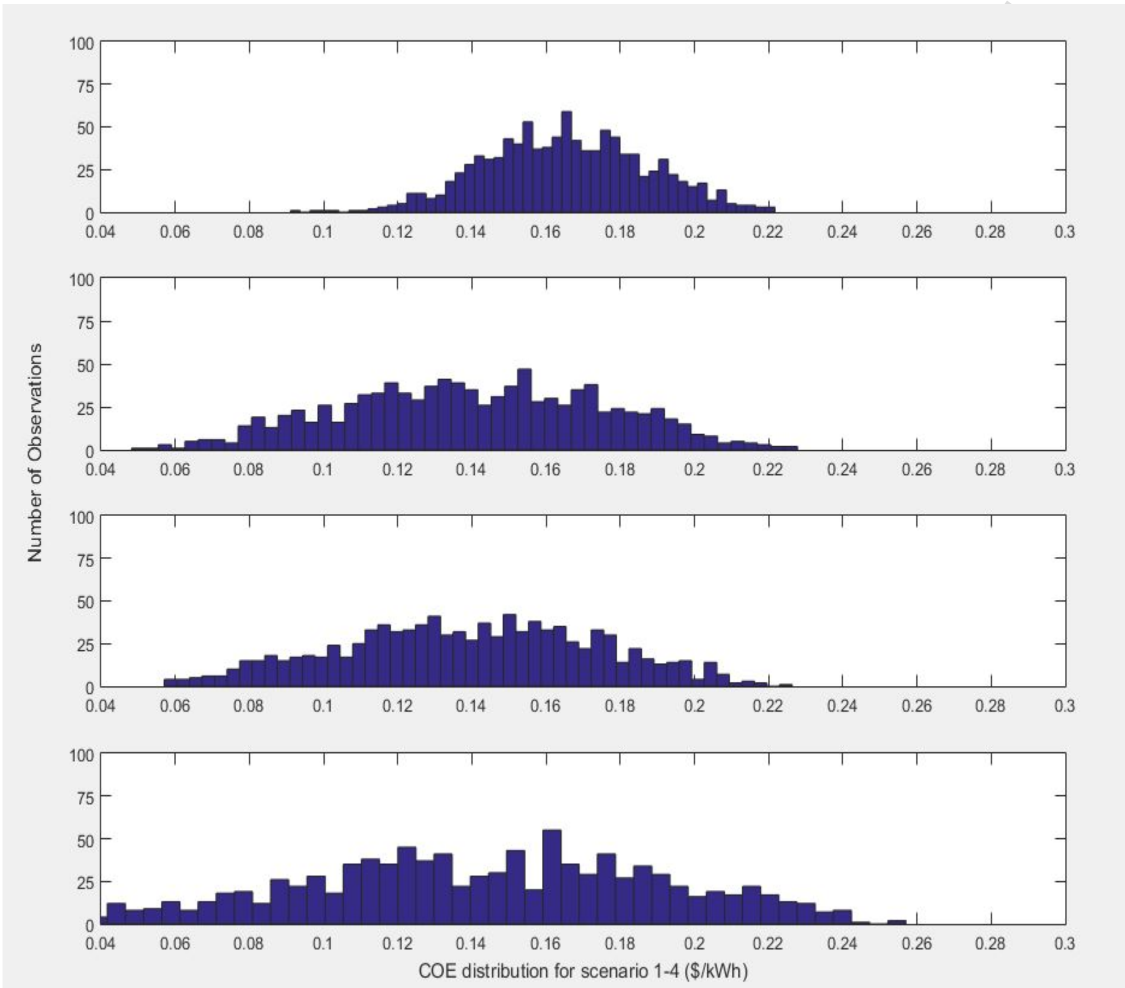

Fig. 19. COE probability distribution of scenario 1-4.

Table 8 shows statistics for these and other important results from the Monte Carlo simulations including descriptive statistics of the scenario distributions, the probabilities associated with any microgrid scenario reaching the optimal situation (deterministic COE), and the probability that any microgrid scenario will be preferred over the conventional utility grid supply (scenario 5). Note that scenario 4 has the highest probability, about 46%, of reaching the optimal COE. There is a better than 28 and 31% chance that the COE of scenarios 2 and 3 are less than or equal to the optimal value. For scenario 1, the probability of achieving the optimal COE is only about 20%., however, the distribution of COE is narrower around the mean. Even with uncertainty in the renewable generation, the microgrid options still yield odds of having lower COE than the utility supply only option (scenario 5) under the assumptions used.

Table 8 COE results from MCS.

Scenario	COE values from MCS ($/kWh)				P(≤ optimum COE)	P(≤ COE of Scenario 5)
	Min	Max	Mean	Range		
1	0.0911	0.2217	0.1653	0.1306	19.80%	96.00%
2	0.0482	0.2278	0.1402	0.1796	28.00%	>99.9%
3	0.0570	0.2263	0.1391	0.1693	30.60%	>99.9%
4	0.0123	0.2570	0.1427	0.2447	45.89%	>99.9%

From the deterministic optimization analysis, scenario 2 has the lowest COE, nevertheless, if all the uncertainty factors are considered, scenario 3 provides the opportunity to achieve the lowest COE overall, albeit with reasonably low probability. With a 4-hour sliding time window, and the large BCHP capacity, any gasifier or engine failure in any but the first hour while the utility TOU electricity price is high, allows the BT and PGS storage to accommodate the lack of BCHP generation. For scenario 2, with the smaller 100 kW BCHP unit and no PGS, accommodation cannot be fully provided by the BT. Scenario 2 is also more dependent on solar energy than scenario 3 and 4, consequently, the uncertainty from solar radiation is reflected in the higher minimum cost for scenario 2. Scenario 4 also shows a much wider range of possible outcomes. To illustrate, the expected COE from scenario 2 is lower than scenario 4, but the odds of achieving that cost are lower. The microgrid design should consider the odds of obtaining performance below expectations and understand the tolerable risk.

3.5. Sensitivity analysis of stochastic variables

Sensitivities of the results are presented for the three main power generation units, BCHP, WT and PV (Table 9). Changing the BCHP capital cost by 15% from the reference value results in average changes of 2.62, 2.00 and 9.87% in the mean COE for scenarios 2-4. When the BCHP O&M cost was changed by 15%, the average changes were 2.82, 4.89 and 6.96% in mean COE for these same scenarios 2-4. It is apparent that the BCHP investment and O&M cost uncertainty is more sensitive in the COE of scenario 4. With respect to the O&M cost, for each scenario, the COE varies by less than 5% indicating that COE is less sensitive to O&M cost category, although BCHP O&M cost is more sensitive than the WT and PV O&M costs.

The variation in wind speed and solar radiation yield greater than 5% change in the final cost for scenario 1, however, solar radiation does not show significant influence on the other scenarios. Therefore, in terms of total cost, the variation in market price is more important than the variations in wind speed and solar irradiance at the site if there is a BCHP on site.

Table 9 Sensitivity analysis of the MCS results.

Case	Mean COE increase/decrease vs. baseline			
	1	2	3	4
+15% BCHP Capital cost	-	2.62%	2.00%	9.87%
+15% WT Capital cost	2.38%	-	-	-
+15% PV Capital cost	2.28%	3.93%	2.34%	9.56%
+15% BCHP O&M cost	-	2.82%	4.89%	6.96%
+15% WT O&M cost	0.00%	-	-	-
+15% PV O&M cost	0.63%	-1.93%	-0.07%	0.92%
+15% Wind speed	-6.36%	-	-	-
+15% Solar irradiance	-7.03%	-3.44%	-0.36%	3.06%

4. Summary and conclusions

A sliding time window optimization modeling approach was applied to the optimal design and dispatch scheduling of a renewable microgrid supplying both heat and electricity. A model microgrid was evaluated with biomass combined heat and power, wind and solar electricity generation, gas-fired boiler, and battery electric, producer gas, and thermal energy storage included.

For the economic assumptions employed, BCHP can significantly improve the cost-efficiency of such a microgrid when compared with utility-supplied grid electricity and natural gas to meet the electrical and heat demands. While for the example location used the mean wind speed was low and wind generation was not selected as optimal, other locations may show superior wind performance. In the optimal scheduling, the inclusion of batteries allows storing electrical energy when utility time of use rates are low and electricity purchase is acceptable, and satisfying demand from storage when the utility rates are high.

Sensitivity analyses show how battery capacity can be optimized. Utility electricity and natural gas prices, as well as energy demand levels all have a significant impact on microgrid design decisions. Cost breakeven points exist for the microgrid against the more conventional utility supply scenario depend on utility pricing, demand, and supply capacities.

The optimum dispatch was evaluated under uncertainty using the probability density functions anticipated for the primary parameters of concern. Monte Carlo simulation was then used to generate the probability distribution of COE as an indicator of risk. The lowest cost option may also have a higher risk of failing to reach the expected design performance. Sensitivity analysis indicated a greater sensitivity to capital cost than the O&M cost for the range of assumptions evaluated. The model provides a means to determine the major risk factors in the microgrid design and weigh the various advantages and disadvantages of each microgrid configuration. Further work will compare optimized scenarios based on both short-term and annual performance and include the uncertainties arising from demand-side management to alter both electricity and heat demand in a combined optimization.

Acknowledgments

Funding for this research was provided by the National Science Foundation through a Partnership for International Research and Education (PIRE) grant. We also gratefully acknowledge the financial support of the China Scholarship Council (CSC).

Reference

[1] Lasseter RH. Microgrids. Power Engineering Society Winter Meeting: IEEE; 2002, p. 305.

[2] Palensky P, Dietrich D. Demand side management: Demand response, intelligent energy systems, and smart loads. IEEE transactions on industrial informatics 2011;7:381.

[3] Hatziargyriou N, Asano H, Iravani R, Marnay C. Microgrids. IEEE Power and Energy 2007;5:78.

[4] Montuori L, Alcázar-Ortega M, Álvarez-Bel C, Domijan A. Integration of renewable energy in microgrids coordinated with demand response resources: Economic evaluation of a biomass gasification plant by Homer Simulator. Applied Energy 2014;132:15.

[5] Acakpovi A, Hagan EB, Michael MB. Cost Benefit Analysis of Self-Optimized Hybrid Solar-Wind-Hydro Electrical Energy Supply as compared to HOMER Optimization. International Journal of Computer Applications 2015;114.

[6] Mamaghani AH, Escandon SAA, Najafi B, Shirazi A, Rinaldi F. Techno-economic feasibility of photovoltaic, wind, diesel and hybrid electrification systems for off-grid rural electrification in Colombia. Renewable Energy 2016;97:293.

[7] Hafez O, Bhattacharya K. Optimal planning and design of a renewable energy based supply system for microgrids. Renewable Energy 2012;45:7.

[8] Castellanos JG, Walker M, Poggio D, Pourkashanian M, Nimmo W. Modelling an off-grid integrated renewable energy system for rural electrification in India using photovoltaics and anaerobic digestion. Renewable Energy 2015;74:390.

[9] Marnay C, Venkataramanan G, Stadler M, Siddiqui AS, Firestone R, Chandran B. Optimal technology selection and operation of commercial-building microgrids. IEEE Transactions on Power Systems 2008;23:975.

[10] Siddiqui AS, Marnay C, Edwards JL, Firestone R, Ghosh S, Stadler M. Effects of carbon tax on microgrid combined heat and power adoption. Journal of Energy Engineering 2005;131:2.

[11] Stadler M, Siddiqui A, Marnay C, Aki H, Lai J. Control of greenhouse gas emissions by optimal DER technology investment and energy management in zero-net-energy buildings. European Transactions on Electrical Power 2011;21:1291.

[12] Sen R, Bhattacharyya SC. Off-grid electricity generation with renewable energy technologies in India: An application of HOMER. Renewable Energy 2014;62:388.

[13] Braslavsky JH, Wall JR, Reedman LJ. Optimal distributed energy resources and the cost of reduced greenhouse gas emissions in a large retail shopping centre. Applied Energy 2015;155:120.

[14] Hawkes A, Leach M. Modelling high level system design and unit commitment for a microgrid. Applied energy 2009;86:1253.

[15] Ren H, Gao W. A MILP model for integrated plan and evaluation of distributed energy systems. Applied Energy 2010;87:1001.

[16] Ren H, Zhou W, Nakagami Ki, Gao W, Wu Q. Multi-objective optimization for the operation of distributed energy systems considering economic and environmental aspects. Applied Energy 2010;87:3642.

[17] Kellogg W, Nehrir M, Venkataramanan G, Gerez V. Generation unit sizing and cost analysis for stand-alone wind, photovoltaic, and hybrid wind/PV systems. IEEE Transactions on energy conversion 1998;13:70.

[18] Zhang D, Shah N, Papageorgiou LG. Efficient energy consumption and operation management in a smart building with microgrid. Energy Conversion and Management 2013;74:209.

[19] Omu A, Choudhary R, Boies A. Distributed energy resource system optimisation using mixed integer linear programming. Energy Policy 2013;61:249.

[20] Marzband M, Ghadimi M, Sumper A, Domínguez-García JL. Experimental validation of a real-time energy management system using multi-period gravitational search algorithm for microgrids in islanded mode. Applied Energy 2014;128:164.
[21] Nwulu NI, Xia X. Optimal dispatch for a microgrid incorporating renewables and demand response. Renewable Energy 2017;101:16.
[22] Zhang D, Evangelisti S, Lettieri P, Papageorgiou LG. Optimal design of CHP-based microgrids: Multiobjective optimisation and life cycle assessment. Energy 2015;85:181.
[23] Wang H, Yin W, Abdollahi E, Lahdelma R, Jiao W. Modelling and optimization of CHP based district heating system with renewable energy production and energy storage. Applied Energy 2015;159:401.
[24] Motevasel M, Seifi AR, Niknam T. Multi-objective energy management of CHP (combined heat and power)-based micro-grid. Energy 2013;51:123.
[25] Moradi MH, Hajinazari M, Jamasb S, Paripour M. An energy management system (EMS) strategy for combined heat and power (CHP) systems based on a hybrid optimization method employing fuzzy programming. Energy 2013;49:86.
[26] Brandoni C, Renzi M. Optimal sizing of hybrid solar micro-CHP systems for the household sector. Applied Thermal Engineering 2015;75:896.
[27] Basu AK, Bhattacharya A, Chowdhury S, Chowdhury S. Planned scheduling for economic power sharing in a CHP-based micro-grid. IEEE Transactions on power systems 2012;27:30.
[28] Basu A, Chowdhury S, Chowdhury S. Operational management of CHP-based microgrid. Power System Technology (POWERCON), 2010 International Conference on: IEEE; 2010, p. 1.
[29] Xu X, Jia H, Wang D, David CY, Chiang H-D. Hierarchical energy management system for multi-source multi-product microgrids. Renewable Energy 2015;78:621.
[30] Moradi MH, Eskandari M. A hybrid method for simultaneous optimization of DG capacity and operational strategy in microgrids considering uncertainty in electricity price forecasting. Renewable Energy 2014;68:697.
[31] Coelho VN, Coelho IM, Coelho BN, Cohen MW, Reis AJ, Silva SM, et al. Multi-objective energy storage power dispatching using plug-in vehicles in a smart-microgrid. Renewable Energy 2016;89:730.
[32] Haddadian H, Noroozian R. Optimal operation of active distribution systems based on microgrid structure. Renewable Energy 2017;104:197.
[33] Baziar A, Kavousi-Fard A. Considering uncertainty in the optimal energy management of renewable micro-grids including storage devices. Renewable Energy 2013;59:158.
[34] Abdullah MA, Muttaqi KM, Agalgaonkar AP. Sustainable energy system design with distributed renewable resources considering economic, environmental and uncertainty aspects. Renewable Energy 2015;78:165.
[35] Neves D, Brito MC, Silva CA. Impact of solar and wind forecast uncertainties on demand response of isolated microgrids. Renewable Energy 2016;87:1003.
[36] Yan X, Abbes D, Francois B. Uncertainty analysis for day ahead power reserve quantification in an urban microgrid including PV generators. Renewable Energy 2017;106:288.
[37] Samimi A, Nikzad M, Siano P. Scenario-based stochastic framework for coupled active and reactive power market in smart distribution systems with demand response programs. Renewable Energy 2017;109:22.
[38] Narayan A, Ponnambalam K. Risk-averse stochastic programming approach for microgrid planning under uncertainty. Renewable Energy 2017;101:399.
[39] Mandelli S, Merlo M, Colombo E. Novel procedure to formulate load profiles for off-grid rural areas. Energy for Sustainable Development 2016;31:130.
[40] Chaudry M, Wu J, Jenkins N. A sequential Monte Carlo model of the combined GB gas and electricity network. Energy Policy 2013;62:473.

[41] Palma-Behnke R, Benavides C, Lanas F, Severino B, Reyes L, Llanos J, et al. A microgrid energy management system based on the rolling horizon strategy. IEEE Transactions on Smart Grid 2013;4:996.
[42] Marietta MP, Graells M, Guerrero JM. A rolling horizon rescheduling strategy for flexible energy in a microgrid. IEEE Energycon: IEEE; 2014, p. 1297.
[43] Fang T, Lahdelma R. Optimization of combined heat and power production with heat storage based on sliding time window method. Applied Energy 2016;162:723.
[44] Wang X, Palazoglu A, El-Farra NH. Operational optimization and demand response of hybrid renewable energy systems. Applied Energy 2015;143:324.
[45] Siqi C, JunYong L, Jiaqi Y, Yaqi N, Yue X, Xin Z, et al. Optimal coordinated operation for microgrid with hybrid energy storage and diesel generator. Power System Technology (POWERCON), 2014 International Conference on: IEEE; 2014, p. 3207.
[46] Pereira M, de la Peña DM, Limon D. Robust economic model predictive control of a community micro-grid. Renewable Energy 2017;100:3.
[47] Wang C, Liu Y, Li X, Guo L, Qiao L, Lu H. Energy management system for stand-alone diesel-wind-biomass microgrid with energy storage system. Energy 2016;97:90.
[48] Jiang B, Fei Y. Smart home in smart microgrid: A cost-effective energy ecosystem with intelligent hierarchical agents. IEEE Transactions on Smart Grid 2015;6:3.
[49] Xie L, Ilic MD. Model predictive economic/environmental dispatch of power systems with intermittent resources. Power & Energy Society General Meeting, 2009 PES'09 IEEE: IEEE; 2009, p. 1.
[50] Silvente J, Kopanos GM, Pistikopoulos EN, Espuña A. A rolling horizon optimization framework for the simultaneous energy supply and demand planning in microgrids. Applied Energy 2015;155:485.
[51] Berg BA, Billoire A. Markov chain monte carlo simulations: Wiley Online Library; 2008.
[52] Bashir M, Sadeh J. Optimal sizing of hybrid wind/photovoltaic/battery considering the uncertainty of wind and photovoltaic power using Monte Carlo. Environment and Electrical Engineering (EEEIC), 2012 11th International Conference on: IEEE; 2012, p. 1081.
[53] Reddy SS. Optimal scheduling of thermal-wind-solar power system with storage. Renewable Energy 2017;101:1357.
[54] Dufo-López R, Cristóbal-Monreal IR, Yusta JM. Stochastic-heuristic methodology for the optimisation of components and control variables of PV-wind-diesel-battery stand-alone systems. Renewable Energy 2016;99:919.
[55] Jahangir H, Ahmadian A, Golkar MA. Optimal design of stand-alone microgrid resources based on proposed Monte-Carlo simulation. Innovative Smart Grid Technologies-Asia: IEEE; 2015, p. 1.
[56] Jenkins BM, Baxter LL, Koppejan J. Biomass combustion. Thermochemical processing of biomass: conversion into fuels, chemicals and power; 2011, p. 13.
[57] Jenkins B, Baxter L, Miles T. Combustion properties of biomass. Fuel processing technology 1998;54:17.
[58] Nguyen DT, Le LB. Optimal energy management for cooperative microgrids with renewable energy resources. Smart Grid Communications (SmartGridComm), 2013 IEEE International Conference on: IEEE; 2013, p. 678.
[59] Talari S, Yazdaninejad M, Haghifam M-R. Stochastic-based scheduling of the microgrid operation including wind turbines, photovoltaic cells, energy storages and responsive loads. IET Generation, Transmission & Distribution 2015;9:1498.
[60] Brum M, Erickson P, Jenkins B, Kornbluth K. A comparative study of district and individual energy systems providing electrical-based heating, cooling, and domestic hot water to a low-energy use residential community. Energy and Buildings 2015;92:306.
[61] Jenkins BM. A comment on the optimal sizing of a biomass utilization facility under constant and variable cost scaling. Biomass and Bioenergy 1997;13:1.
[62] Silvente J, Aguirre A, Crexells G, Zamarripa M, Méndez C, Graells M, et al. Hybrid time representation for the scheduling of energy supply and demand in smart grids. Comput Aided Chem Eng 2013;32:553.

[63] Wickwire S. Biomass Combined Heat and Power catalog of technologies. Washington, DC 2007;1:10.

[64] DiOrio N, Dobos A, Janzou S. Economic Analysis Case Studies of Battery Energy Storage with SAM. National Renewable Energy Lab.(NREL), Golden, CO; 2015.

[65] Tidball R, Bluestein J, Rodriguez N, Knoke S. Cost and performance assumptions for modeling electricity generation technologies. ICF International, Fairfax, VA; 2010, p. 275.

[66] Energy Metering (NEM) Available: http://www.cpuc.ca.gov/General.aspx?id=3800Net [Accessed: October 2016].

- A model was developed to optimize the design of a biomass-integrated renewable energy microgrid employing combined heat and power with energy storage.
- A receding horizon optimization with Monte Carlo simulation was proposed to evaluate optimal microgrid design and dispatch under uncertainty.
- The model application provides a means to determine major risk factors associated with alternative design integration and operating strategies.